

## Highly charged ion beam applied to lithography technique (invited)<sup>a)</sup>

Sadao Momota and Yoichi Nojiri

*Kochi University of Technology, Miyano-kuchi, Tosayamada-cho, Kami, Kochi 782-8502, Japan*

Jun Taniguchi and Iwao Miyamoto

*Tokyo University of Science, 2641 Yamasaki, Noda, 278-8501 Chiba, Japan*

Noboru Morita

*University of Toyama, 3190 Gofuku, Toyama 930-8555, Japan*

Noritaka Kawasegi

*Toyama Industrial Tech. Center, 150, Futagami-machi, Takaoka, Toyama 933-0981, Japan*

(Presented 30 August 2007; received 30 August 2007; accepted 18 December 2007; published online 20 February 2008)

In various fields of nanotechnology, the importance of nanoscale three-dimensional (3D) structures is increasing. In order to develop an efficient process to fabricate nanoscale 3D structures, we have applied highly charged ion (HCI) beams to the ion-beam lithography (IBL) technique. Ar-ion beams with various charge states (1+ to 9+) were applied to fabricate spin on glass (SOG) and Si by means of the IBL technique. The Ar ions were prepared by a facility built at Kochi University of Technology, which includes an electron cyclotron resonance ion source (NANOGAN, 10 GHz). IBL fabrication was performed as a function of not only the charge state but also the energy and the dose of Ar ions. The present results show that the application of an Ar<sup>9+</sup> beam reduces the etching time for SOG and enhances the etching depth compared with those observed with Ar ions in lower charged states. Considering the high-energy deposition of HCI at a surface, the former phenomena can be understood consistently. Also, the latter phenomena can be understood based on anomalously deep structural changes, which are remarkable for glasses. Furthermore, it has also been shown that the etching depth can be easily controlled with the kinetic energy of the Ar ions. These results show the possibilities of the IBL technique with HCI beams in the field of nanoscale 3D fabrication. © 2008 American Institute of Physics. [DOI: 10.1063/1.2834317]

### INTRODUCTION

The lithography technique is one of the popular and powerful tools to perform micronanoscale fabrication. For example, the development of the lithography technique has made it possible to perform the mass production of large-scale integration on which a circuit pattern is drawn with a scale of 100 nm or smaller. Recently, the importance of nanoscale three-dimensional (3D) structures is increasing in various fields of industrial applications, such as microelectromechanical system, optical devices, and biology. Therefore, the development of a fabrication process to produce nanoscale 3D structures is now eagerly required. The ion beam has smaller lateral straggling and better controllability of the range distribution in materials compared with using photons or electrons. These properties suggest that the ion-beam lithography (IBL) technique would be a hopeful candidate to fabricate nanoscale 3D structures. In order to promote the application of the IBL technique to this field, we have applied highly charged ion (HCI) beams to the IBL technique.

A series of previous studies have shown a high reactivity of HCI with materials compared with singly charged ions.<sup>1</sup> Considering the high reactivity, various kinds of applications

have been proposed, as summarized in Ref. 2. The development of HCI sources has stimulated efforts to apply HCI beams to industry. For example, the Xe<sup>44+</sup> was applied to the IBL technique to fabricate polymethyl methacrylate<sup>3</sup> and a self-assembled monolayer.<sup>4</sup> Although an enhancement of the irradiation effect of HCI beams, which is caused by their high reactivity, was successfully confirmed in those studies, detailed natures of the lithography process have not yet been studied. Although HCI has a high efficiency for acceleration by means of an electric field to obtain a higher energy compared with singly charged ion, the depths of structures fabricated in the above-mentioned studies have been 200 nm or

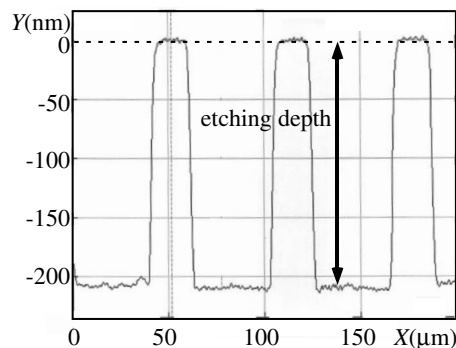


FIG. 1. Typical surface profile of SOG fabricated by IBL. The dose of Ar<sup>1+</sup> ion is  $4.7 \times 10^{14}$  ions/cm<sup>2</sup> and the etching time is 180 s.

<sup>a)</sup> Invited paper, published as part of the Proceedings of the 12th International Conference on Ion Sources, Jeju, Korea, August 2007.

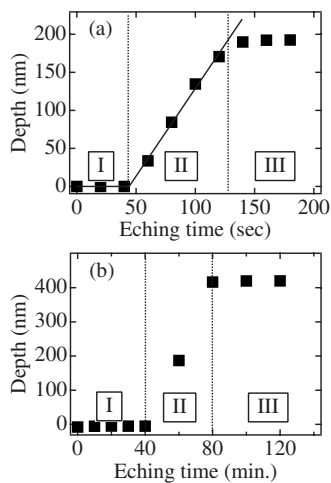


FIG. 2. Etching depth as a function of the etching time. The time evolution of the etching processes for SOG and Si are shown. (a)  $Ar^{1+}$  ion with 90 keV was irradiated on SOG. The dose of Ar ions was  $6.3 \times 10^{13}$  ions/cm<sup>2</sup>. The solid line shows the fitting result with Eq. (1). (b)  $Ar^{4+}$  ion with 240 keV was irradiated on Si. The dose of Ar ions was  $1.3 \times 10^{15}$  ions/cm<sup>2</sup>.

shallower. In this article, the effectiveness of HCI beams in the IBL technique is discussed based on detailed observations of fabrication process while changing not only the charge state but also the dose and the energy of the ions. Furthermore, by comparing the results for amorphous and crystalline materials, the material dependence of the HCI effect is briefly discussed. For the present research, the ECR ion source is suitable to produce HCI beams with a sufficiently high beam intensity to perform IBL.

## EXPERIMENTAL

Ar ions with various charge states (1+ to 9+) were irradiated onto materials to be fabricated by using a facility built at Kochi University of Technology.<sup>5</sup> The Ar ions were prepared by a 10 GHz NANOGAN,<sup>6</sup> which is an ECR ion source. Accelerated Ar ions were identified and separated by using a dipole magnet. Separated Ar ions were irradiated onto spin-on-glass (SOG) and single-crystal Si at room temperature. In the present study, accuglass 512B applied on a Si substrate was used as SOG. In order to extract the detailed character of the fabrication process, it was observed as a function of not only the charge state but also the dose and the energy of the Ar ions. In order to fabricate a pattern on

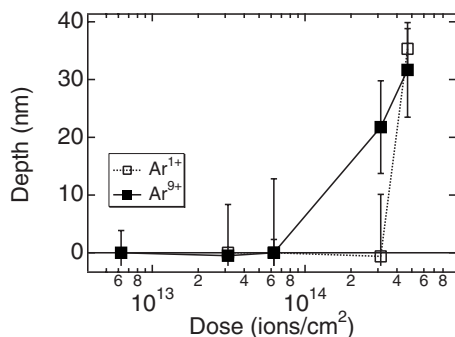


FIG. 3. Depth of concave structures fabricated on SOG by sputtering as a function of the dose of Ar ions.

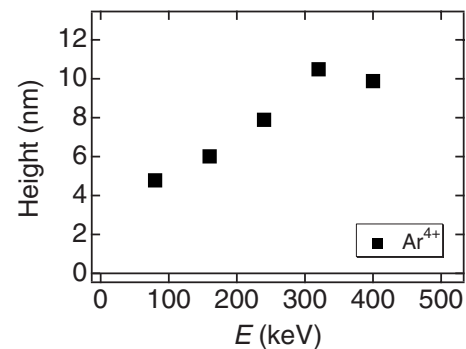


FIG. 4. Height of hillock structures fabricated on Si by irradiation-induced amorphization as a function of the energy of  $Ar^{4+}$  ion.

irradiated materials, Ar ions were irradiated through a Cu stencil mask, which had square holes with  $43 \mu\text{m}$  sides. The irradiation rate was monitored as a target current during the irradiation process. The typical irradiation rates for Ar ions were  $0.1\text{--}1 \mu\text{A}/\text{cm}^2$ .

The etching process followed after the irradiation process. Irradiated SOG and Si were etched at room temperature in a solution of BHF and HF, respectively. The surface profile of SOG (Si) was examined using an alpha step IQ profilometer (atomic force microscopy) every 20 s (10 min) up to 180 s (120 min). In order to complete the etching process, irradiated Si was subsequently etched in HF for 24 h. Details about the IBL process and measurements are shown in Refs. 7 and 8.

## RESULTS AND DISCUSSION

The Cu stencil mask pattern was successfully transferred to SOG and Si by performing IBL with Ar-ion beams, and the irradiated region became a concave structure, as shown in Fig. 1. The irradiation of Ar ions enhanced the etching rate both of SOG and Si. The bottom of the concave structure was relatively flat, and the fabrication depth was simply defined to be the distance between the top and bottom of the concave structure.

The etching depth was observed as a function of the etching time for SOG and Si, as shown in Figs. 2(a) and 2(b), respectively. The time scale of the etching process is one or more orders faster for SOG compared with Si. In principle, the etching process consists of three phases as shown in the figures. In the first phase (I), the concave structure on the irradiated surface does not grow. The fabrication caused by

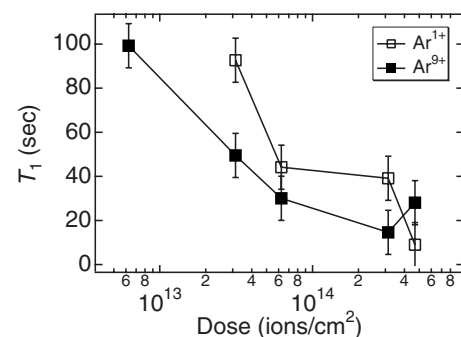
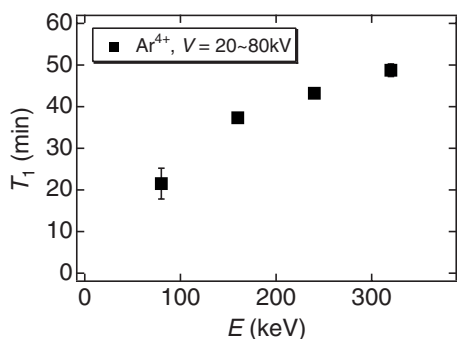


FIG. 5.  $T_1$  for SOG as a function of the dose of Ar ions.

FIG. 6.  $T_1$  for Si as a function of the energy of Ar ions.

an etching process starts, and the concave structure grows in the second phase (II). Finally, the concave structure stops growing in the third phase (III). Considering phase I, the existence of a resistant layer for etching is expected at the top surface. In order to analyze the relation between the etching depth ( $D$ ) and the etching time ( $t$ ) numerically, the time evolution of the etching process is analyzed with a function given by

$$D = k_0 \quad \text{if } t < T_1,$$

$$= k_0 + k_1(t - T_1) \quad \text{if } T_1 \leq t \leq T_2, \quad (1)$$

where  $T_1$  ( $T_2$ ) is the time to start (stop) etching.

The depth of structures fabricated only by the irradiation process,  $k_0$ , is positive (concave structures) for SOG and negative (hillock structures) for Si. In the case of SOG, it is expected that concave structures are fabricated by the sputtering process, and the structures grows with the dose of Ar ions, as shown in Fig. 3. Furthermore, the growth of concave structures is promoted by  $\text{Ar}^{9+}$  compared with  $\text{Ar}^{1+}$ . It is implied from this result that a HCl beam would enhance the sputtering process for SOG. The formation of hillock structures on the Si surface suggests that the irradiation-induced amorphization effect on Si, which causes volume expansion, occurs prior to the sputtering process at the first stage of ion-beam irradiation. Also, the height of hillock structures increases with the energy of the Ar ion, as shown in Fig. 4. This phenomenon can be understood by an extension of the amorphized layer to a deeper region for a high-energy beam. Concerning the etching start time,  $T_1$  decreases with the dose of Ar ions for SOG, as shown in Fig. 5. This tendency observed in  $T_1$  is remarkable for  $\text{Ar}^{9+}$ , compared with  $\text{Ar}^{1+}$ . The results support the previous idea that the top layer, which is

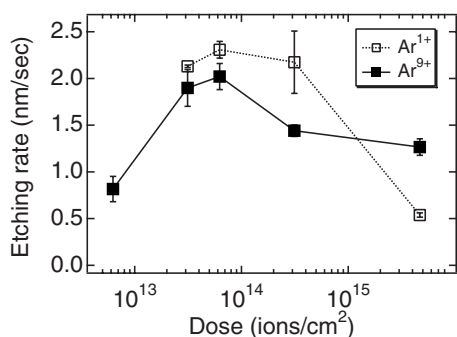
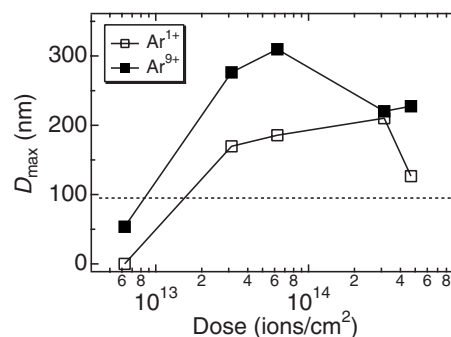
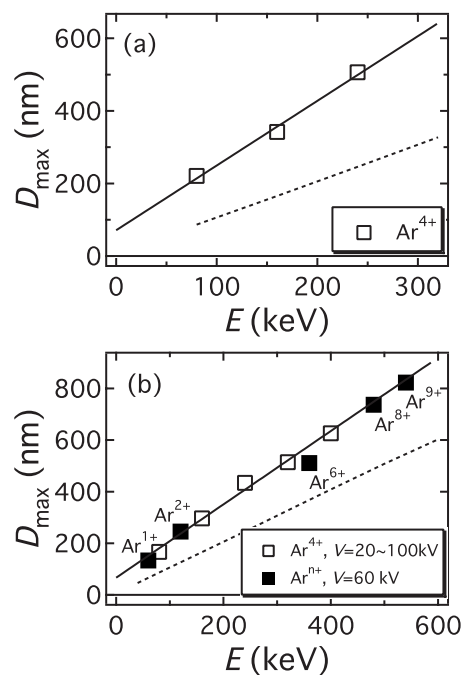


FIG. 7. Etching rate of SOG as a function of the dose of Ar ions.

FIG. 8.  $D_{\max}$  of SOG as a function of the dose of Ar ions. The broken line shows the range of Ar ions with 90 keV in  $\text{SiO}_2$  (95 nm), calculated by the SRIM code.

resistant to etching, is removed by the sputtering process for SOG. Also, the promoted removal of the etching-resistant layer on the SOG surface would induce a decrease in  $T_1$  observed with  $\text{Ar}^{9+}$ . In the case of Si,  $T_1$  increases with the energy of Ar ions, as shown in Fig. 6. The decrease in the energy deposition of Ar ions at the top layer of Si suppresses the irradiation-induced amorphization effect, and the time to remove the top layer by the etching process becomes longer. The etching rate,  $k_1$ , observed with SOG as a function of the dose of Ar ions is shown in Fig. 7. In this figure, the optimized etching rate of SOG is found at a dose of  $6 \times 10^{13}$  ions/cm<sup>2</sup> to be about 2 nm/s, and does not depend on the charge state. The maximum etching depth,  $D_{\max}$ , is defined by the etching depth observed at  $t=180$  s and 24 h for SOG and Si, respectively.  $D_{\max}$  of SOG is optimized at a dose of  $\sim 1 \times 10^{14}$  ions/cm<sup>2</sup> for  $\text{Ar}^{1+}$  and  $\text{Ar}^{9+}$ , as shown in Fig. 8.  $D_{\max}$  is two times deeper for  $\text{Ar}^{1+}$  and three times deeper for  $\text{Ar}^{9+}$ , compared with the range of Ar ions calcu-

FIG. 9.  $D_{\max}$  of (a) SOG and (b) Si as a function of the energy of Ar ions. The solid lines show the fitting results with a linear function, and the broken lines show the range of Ar ions in  $\text{SiO}_2$ , calculated by the SRIM code. In (b), the energy dependence observed by changing charge states is also shown.

lated by the SRIM code.<sup>9</sup> The obvious extension of  $D_{\max}$  might be understood based on an anomalously deep structural change caused by an indirect irradiation effect, such as irradiation-induced shock waves, or an enhancement of their amplitude, as mentioned in Ref. 10. It was also mentioned that this long-range action effect is remarkable for glasses in Ref. 10. In the case of SOG, enhanced energy deposition at the surface would stimulate not only the sputtering process but also the long-range action effect.

$D_{\max}$  increases linearly with the beam energy of Ar ions for SOG and Si, as shown in Figs. 9(a) and 9(b). In these figures,  $D_{\max}$  is two times deeper compared with the calculated Ar range, which is comparable with SOG irradiated by Ar<sup>1+</sup> ions. Also, no significant charge state dependences are found for Si. Although  $D_{\max}$  increases with the beam energy of Ar ions, the etching start time becomes longer, as shown in Fig. 6. The irradiation-induced amorphization effect will suppress this delay of the etching process. The amorphization effect will be promoted by the irradiation of ions in a higher charge state, or by an additional irradiation of low-energy Ar ions, which induce higher energy deposition at the surface.

## CONCLUSION

In this study, HCI beams of Ar were applied to the IBL technique to fabricate SOG and Si. It is concluded from the present results that HCI beams reduce the etching time because of the removal of an etching-resistant layer at the sur-

face stimulated by high-energy deposition. Also, the long-range action effect enhances the fabrication depth, and this effect is remarkable for SOG compared with Si. Furthermore, it was shown that the fabrication depth could be easily controlled to a precision of 10 nm by changing the charge state as well as the acceleration voltage. All of these results show the high feasibility of HCI beams to apply the IBL technique to fabricate nanoscale 3D structures.

<sup>1</sup>J.-P. Briand, G. Giardino, G. Borsoni, V. Le Roux, N. Béchu, S. Dreuil, O. Tüske, and G. Machicoane, *Rev. Sci. Instrum.* **71**, 627 (2000).

<sup>2</sup>U. Kentsch, S. Landgraf, M. Schmidt, H. Tyrroff, G. Zschornack, F. Grossmann, V. P. Ovsyannikov, and F. Ullmann, *Nucl. Instrum. Methods Phys. Res. B* **216**, 196 (2004).

<sup>3</sup>J. D. Gillaspay, D. C. Parks, and L. P. Ratliff, *J. Vac. Sci. Technol. B* **16**, 3294 (1998).

<sup>4</sup>L. P. Ratliff, R. Minniti, A. Bard, E. W. Bell, J. D. Gillaspay, D. Parks, A. J. Black, and G. M. Whitesides, *Appl. Phys. Lett.* **75**, 590 (1999).

<sup>5</sup>S. Momota, Y. Nojiri, M. Saihara, A. Sakamoto, H. Hamagawa, and K. Hamaguchi, *Rev. Sci. Instrum.* **75**, 1497 (2004).

<sup>6</sup>P. Sortias, M. Bisch, P. Bricault, P. Leherissier, M. Lewitowicz, R. Leroy, C. F. Liang, J. Y. Pacquet, P. Daris, J. P. Puteaux, J. Olert, J. P. Rateau, and M. G. Saintlaurent, *Proceedings of the 11th International Workshop on ECR Ion Sources, Groningen, 1993* (unpublished), p. 97.

<sup>7</sup>S. Iwamitsu, M. Nagao, S. A. Pahlovy, K. Nishimura, M. Kashihara, S. Momota, Y. Nojiri, J. Taniguchi, I. Miyamoto, T. Nakao, N. Morita, and N. Kawasegi, *Colloids Surf., A* **313-314**, 407 (2008).

<sup>8</sup>N. Kawasegi, N. Morita, S. Yamada, N. Takano T. Oyama, S. Momota, J. Taniguchi, and I. Miyamoto, *Appl. Surf. Sci.* **253**, 3284 (2007).

<sup>9</sup>J. F. Ziegler, *The Stopping and Range of Ions in Matter* (Pergamon, New York, 1985).

<sup>10</sup>A. Deshkovskaya, *Nucl. Instrum. Methods Phys. Res. B* **166-167**, 511 (2000).